Steady, Symmetric, and Reversible Growth and Dissolution of Individual Amyloid-β Fibrils

Yuechuan Xu,[1] Mohammad S. Safari,[1] Wenchuan Ma,[1] Nicholas P. Schafer,[2,3] Peter G. Wolynes,[2,3,*] and Peter G. Vekilov[1,4,*]

[1]*Department of Chemical and Biomolecular Engineering, University of Houston, 4726 Calhoun Road, Houston, TX 77204-4004, USA*

[2]*Center for Theoretical Biological Physics, Rice University, P.O. Box 1892, MS 654, Houston, TX 77251-1892, USA*

[3]*Department of Chemistry, Rice University, P.O. Box 1892, MS 60, Houston, TX 77251-1892, USA*

[4]*Department of Chemistry, University of Houston, 3585 Cullen Blvd., Houston, TX 77204-5003, USA*

Abstract. Oligomers and fibrils of the amyloid-β (Aβ) peptide are implicated in the pathology of Alzheimer's disease. Here, we monitor the growth of individual Aβ40 fibrils by time-resolved *in situ* atomic force microscopy and thereby directly measure fibril growth rates. The measured growth rates in a population of fibrils that includes both single protofilaments and bundles of filaments are independent of the fibril thickness, indicating that cooperation between adjacent protofilaments does not affect incorporation of monomers. The opposite ends of individual fibrils grow at similar rates. In contrast to the "stop-and-go" kinetics that has previously been observed for amyloid-forming peptides, growth and dissolution of the Aβ40 fibrils are relatively steady for peptide concentration of 0 – 10 μM. The fibrils readily dissolve in quiescent peptide-free solutions at a rate that is consistent with the microscopic reversibility of growth and dissolution. Importantly, the bimolecular rate coefficient for the association of a monomer to the fibril end is significantly smaller than the diffusion limit, implying that the transition state for incorporation of a monomer into a fibril is associated with a relatively high free energy.

KEYWORDS

amyloid fibrillization; fibril growth; Abeta solubility; fibrillization rate constant.

TOC GRAPHIC

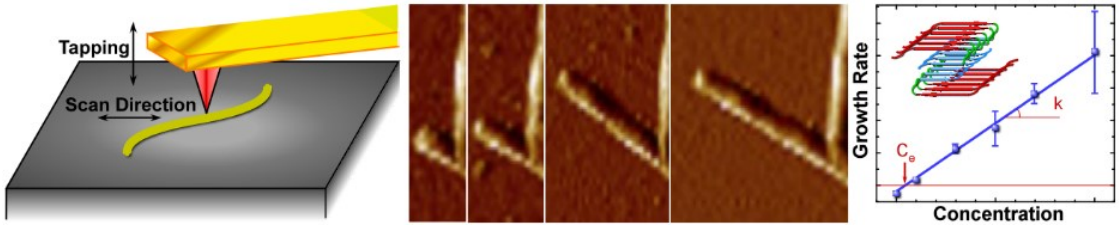

INTRODUCTION

The hallmark pathology of Alzheimer's disease (AD) is the accumulation of plaques of the protein fragment amyloid-β (Aβ) outside neurons in the brain.[1] Accordingly, the amyloid cascade hypothesis states that cerebral amyloid deposition may represent a critical pathogenic event in Alzheimer's.[2-4] Despite a recent interest in neurotoxic Aβ oligomers,[5-12] the correlation of Aβ fibrils and plaques to AD is still actively scrutinized.[13-39] Aβ forms a variety of stable and structurally disparate amyloid fibrils both *in vivo* and *in vitro*.[13, 35, 40] Distinct fibril structures have been linked to divergent clinical outcomes.[13] Emerging evidence suggests that fibrils of Aβ polymorphs that form in the presence of lipid membranes, which are abundant *in vivo*, may be highly neurotoxic.[41-43] Furthermore, in early-onset familial forms of AD,[44] especially those associated with the Arctic[45] and Iowa[46] variants of Aβ, it is generally accepted that extensive fibrillization of mutant Aβ is the primary cause of cerebral amyloid angiopathy.[47] In addition, even though the structures of the toxic oligomers may be distinct from those of mature fibrils, understanding the molecular-level processes of fibril growth may be informative of oligomer behaviors and must play a part in the systems biology.[13, 26, 40, 48-51]

Here we explore the growth of Aβ40 fibrils. Two Aβ peptide isoforms, comprised, respectively, of 40 or 42 aminoacid residues, dominate the population of polypeptide chains generated by cleaving the amyloid precursor protein.[52-53] Both peptides fibrilize *in vivo* and *in vitro*; Aβ42 aggregates faster at comparable concentrations,[54-55] but the differences in aggregation kinetics are not large.[13] The shorter peptide, Aβ40, is present at 5-to-10-fold higher concentrations than Aβ42[56] and is overrepresented in mature fibrils and plaques.[57]

The kinetics of amyloid assembly have typically been investigated in bulk assays,[58-60] in which the recorded signal reflects a convolution of molecularly distinct events: nucleation, growth, fragmentation, and fibril surface-catalyzed nucleation. It is hard to disentangle these processes.[61] Recently, valuable insights have come from studies focused on the growth of individual amyloid fibrils, observed by atomic force microscopy (AFM)[14, 61-66] and fluorescence microscopy.[67-71] These studies have raised several questions concerning the mechanisms of Aβ40 fibril growth. Is fibril growth steady or do periods of stagnation alternate with bursts of growth? Do parallel adjacent protofilaments cooperate to grow faster or slower than isolated ones? Do opposing fibril ends grow at similar rates in a symmetrical fashion? Do fibrils grow by incorporation of monomers or of dimers and higher oligomers? Is the sequence of molecular-level events leading to incorporation in a fibril exactly reversed during dissolution? Is the incorporation of Aβ monomers in a fibril delayed by a kinetic barrier or is its rate limited only by monomer diffusion?

Here we monitor the growth of individual Aβ40 fibrils by time-resolved *in situ* AFM to address these questions.

RESULTS AND DISCUSSION

Determination of fibril growth rates. We generate fibrils in a stirred solution and deposit them on freshly cleaved mica surfaces[72] mounted on the AFM scanner; please see the Methods section below. We fill the AFM fluid cell with an Aβ40 solution of known concentration in 40 mM phosphate buffer at pH = 7.4. The solution is replenished periodically to maintain constant peptide concentration. We employ the tapping mode of AFM, whereby the substrate, on which the fibrils are deposited, is scanned with an oscillating tip (Fig. 1A). The amplitude, the resonance frequency, and the phase shift of the tip vibrations are modulated by the interaction with the fibril and the response is used to deduce its topography.[73] AFM imaging of the mica surface in this solution reveals fibrils firmly attached to the substrate.[74] In time, both ends of the fibrils grow (Fig. 1 B – E). We select immobile markers on the substrate that are visible in several consecutive images and use them as reference points to measure the displacement of each fibril end along the fibril axis (Fig. 1 B – E). We evaluate the fibril growth rate as the slope of the time correlation of the fibril end displacement (Fig. 1F). As defined, the growth rate characterizes individual fibrils and can be determined uniquely for each of the two fibril ends.

The fibril growth rate measurements described above are direct. They do not require fluorescent labeling of the peptide or the presence of fluorophores such as Thioflavin T, both of which could modify the aggregation kinetics and thermodynamics. To address the concern that scanning with the AFM tip might influence fibril growth we examined the impact of the imaging tip and solution shear due to the horizontal motion of the AFM tip in the immediate vicinity of the surface. We found that several changes in scan protocol do not affect the apparent rates of fibril growth. Tip velocities of 1 to 10 $\mu m\ s^{-1}$ would engender a boundary layer around the tip with thickness of the order of a few microns[75] in which the shear rates are of the order of 1 to 10 s^{-1}. Higher solution shear may affect the conformation of unfolding globular proteins[76-78] and may to a lesser extent impact the conformation of Aβ monomers (in solution, Aβ(1–40) adopts a structure

with α-helical and hairpin segments).[19, 48, 79-80] The resulting conformational variability may enhance or suppress the fibrillization rates, similar to observations with other protein condensates.[81-82]

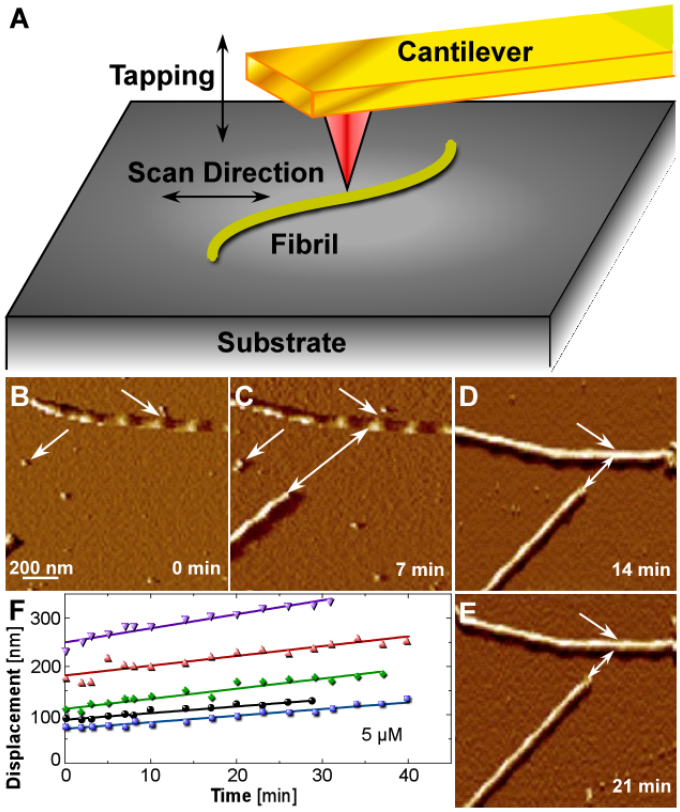

Figure 1. Determination of growth rates for individual Aβ40 fibrils. A. Schematic of tapping-mode imaging of a fibril deposited on a substrate by an AFM tip. **B-E.** Time-resolved *in situ* AFM images showing the growth of an Aβ40 fibril in a 1 μM solution. White arrows indicate immobile reference points. Double-sided arrows indicate distance between a fibril end and a reference point. Image acquisition times were about 100 s. **F.** Evolutions of the displacements of five fibril ends and the respective best-fit lines that were used to determine the fibril growth rates at a solution concentration of 5 μM, as indicated in plot.

Our tests showed, however, that scanning in two perpendicular directions (Fig. 2A) produced statistically indistinguishable growth rates (Fig. 2B). In a second test, we increased the tip velocity from 2 to 10 μm s^{-1} by varying the image size and scan rate. We analyzed the similarity between the distributions of growth rates obtained with distinct tip velocities (Fig. 2C) by one-

way analysis of variance (ANOVA), a statistical procedure, which compares the variance between the three groups to the variance within each group of data. The F value, corresponding to the ratio of the two variances, is 1.55, smaller than the critical value of 3.15 for three groups consisting of 65 independent measurements. The p value was 0.22, greater than the significance level of 0.05, certifying that the hypothesis of equality of the three mean growth rates is held. All measurements discussed below were executed with scanning tip velocities between 5 and 10 μm s^{-1}. In a third test, we compared the fibril growth rates in an area of the substrate that was continuously imaged for 13 min, to those of fibrils outside of the viewing area (Fig. 2 D – G). The growth rates in both groups were in the range 3 – 5 pm s^{-1}. As evidence that interaction with the substrate does not modify the growth rates, below we highlight the similarity of the growth rates measured using the present method to those determined from time-dependent bulk growth of fibrils in solution.[14]

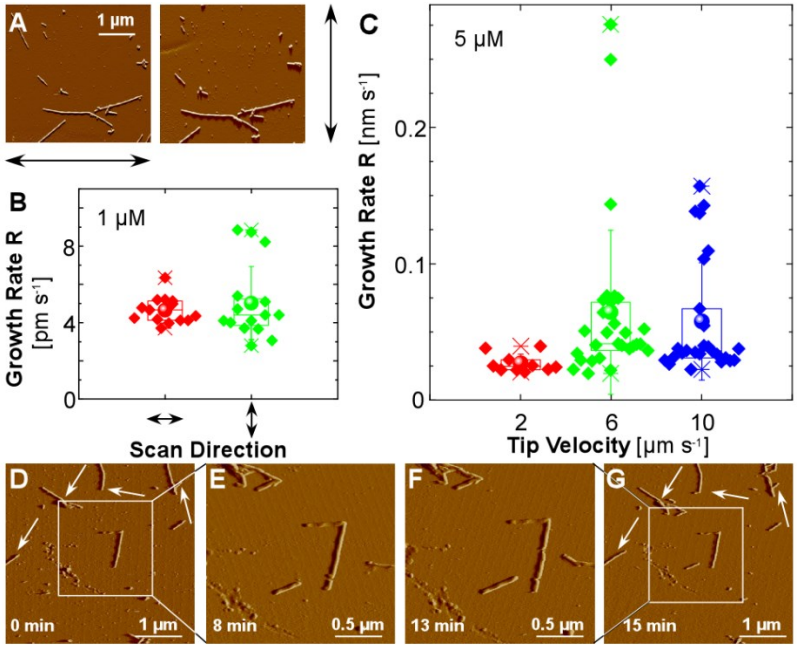

Figure 2. Tests for imaging artefacts. A. *In situ* AFM images showing fibrils growing in 1 μM Aβ40 solution scanned in directions indicated by double-sided arrows. **B.** Jitter plots of fibril growth rates determined from images collected with the two perpendicular scanning directions shown in A. Upper, median, and lower horizontal lines exceed 75, 50, and 25% of the data points, respectively. × indicate fastest and slowest growth rates, ● mark the average values, capped vertical bars denote the standard deviations of the data sets. **C.** Jitter plots of distributions of fibril growth rates at displayed Aβ40 concentration, determined using indicated tip velocities. **D-G.** Time-resolved *in situ* AFM images showing the growth of Aβ40 fibrils in a 1 μM solution over 15

min employing embedded scan areas. Tip velocity 5 μm s^{-1}. White box indicates area of zoom-in scans in E and F after image in D was recorded. **G.** Image with lower zoom ratio incorporates area scanned in E and F, highlighted in white box. Arrows in D and G indicate fibrils that grew outside of continuously scanned area observed in E and F. Image acquisition times in A and D – G were about 100 s.

Fibril polymorphism, growth symmetry, and growth rate variability. Aβ forms several stable distinct polymorph structures both *in vivo* and *in vitro*.[13, 35, 40, 83] In most of the studied structures, the constituent monomers fold into a U-contour with sides comprised of β-strands.[14, 40, 84-87] The monomers assemble into a gutter-shaped protofilament with walls formed by β-sheets, in which the constituent β-strands align perpendicular to the long protofilament axis.[40, 88] The assembly of two or three parallel protofilaments is classified as a filament and a single fibril often contains several filaments.[88] All elements of this structural hierarchy may attain various morphologies.[14, 26, 40, 84] Whereas Aβ oligomers may contain antiparallel β-strands,[48] abundant evidence suggests that the protofilaments found in mature fibrils are built as parallel β-sheets.[14, 26, 40, 89-90] The two most common structures formed *in vitro* consist of either two or three symmetrically arranged protofilaments running parallel to the fibril axis.[14, 26, 40, 84] The threefold symmetric filaments, whose thickness is about 7.0 nm, dominate in quiescent solutions, whereas agitated solutions (like those we use to make our samples) promote a twofold symmetric polymorph (as in Fig. 3A), in which the filaments have a roughly rectangular cross-section with dimensions 6 × 5.2 nm^2.[14, 40, 84] Importantly, the structure of a fibril does not change along its length. Morphological characteristics, such as fibril width, twist period, and mass-per-length, propagate as the fibril grows and transfer from a seed to the newly grown segments.[40]

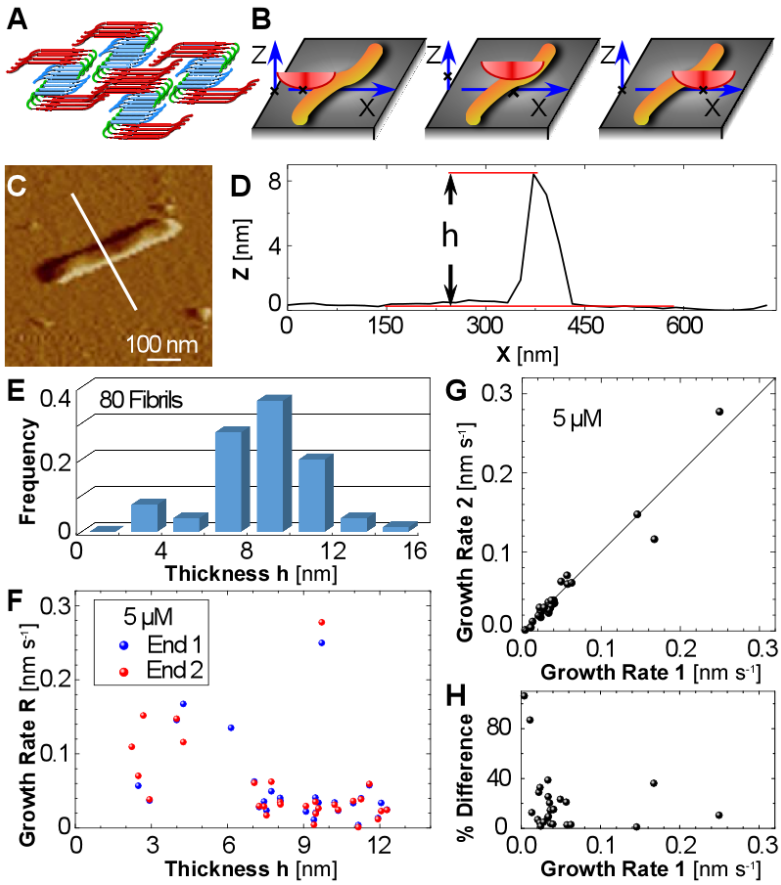

Figure 3. The fibril thickness and symmetry of growth of two fibril ends. A. Schematic of a fibril that consists of four filaments, each comprised of two protofilaments related by a twofold axis. Red, green, and blue denote N-terminus, hinge, and C-terminus of the Aβ40 peptide. **B.** Schematic of the interaction of an AFM tip with a fibril. X axis extends along scan direction, z axis measures separation of tip from substrate. × mark the readouts along the z and x axes when the tip touches the fibril, when the tip is on top of the fibril, and when the tip detaches from the other side of the fibril, respectively. **C and D.** Illustration of measurement of fibril thickness using AFM. **C.** Height mode image of a fibril growing at Aβ40 concentration 1 μM. **D.** Height profile along line in A and illustration of thickness *h* determination. **E.** Distribution of fibril thicknesses. **F.** Growth rates of opposing fibril ends plotted as a function of respective fibril thickness. Solution concentration is indicated in the plot. **G.** Correlation between rates of growth of the two fibrils ends. Three points corresponding to fibrils that only display one end in the AFM field of view have been omitted from this plot. Solution concentration is indicated in the plot. **H.** Magnitude of the relative discrepancy between the growth rates of the two fibril ends in G.

The width of a fibril rendered by AFM is a convolution of the shapes of the fibril and the AFM tip (Fig. 3B).[73, 91-92] The thickness of the fibril, however, determined as the deviation from the height level of the mica substrate (Fig. 3 B – D), does not suffer from similar exaggeration. We observe that the distribution of the fibrils thicknesses is bimodal, with maxima at 3 and 9 nm (Fig.

3E). The lower value is less than the filament thicknesses of both the threefold and twofold Aβ40 polymorphs but is comparable to the height of a single U-shaped protofilament;[14, 40, 84] fibrils consisting of single protofilaments with mass-to-length ratio of about 9 kDa nm^{-1} (corresponding to a single chain of monomers with molecular weight 4.33 kDa and spacing of 0.47 nm)[84, 93-95] have been observed in populations of both polymorphs.[87] Consistent with expectations for seeds generated in stirred solutions[14] and the propagation of fibril structure from seed to new growth[40] we conclude that the thinnest fibrils in our experiments represent stand-alone protofilaments of the twofold symmetric polymorph. Evidence discussed below indicates that the thicker fibrils that we observe are likely bundles of filaments of this same twofold symmetric polymorph.

If protofilaments within the same fibril grow sufficiently fast so as to compete for a supply of monomers from the solution, then we would expect decreasing fibril growth rate as fibril thickness increases. The independence of the fibril growth rate of the fibril thickness (Figs. 3F, S7 and S8; the linear correlation coefficients for the $R(h)$, $R(h^{-1})$, and $R(h^{-2})$ dependences are, respectively, 0.09, 0.03, and 0.10) indicates that the convective-diffusive supply of monomers to the fibril end is not a rate-determining step of growth, in contrast to significantly faster (ca. 10,000-fold) growing sickle cell hemoglobin polymers.[96-97] Importantly, this independence indicates that adjacent protofilaments do not cooperate to assist or hamper monomer incorporation into their respective tips. Thus, models of Aβ40 aggregation assuming single protofilaments [15, 19, 48] are likely to predict adequately the growth dynamics of fibrils comprised of multiple protofilaments.

The opposing ends of the majority of the monitored fibrils grow with rates that differ by less than 40% (Fig. 3 G and H) and the magnitude of this difference is independent of the growth rate (Fig. 3H, the linear correlation coefficient is 0.002). The differences of the rates between the opposing fibril ends are within the range of variability of the growth rates of individual fibril ends (see, e.g., Fig. 2B). This approximate growth rate symmetry contrasts with previous

measurements of the growth dynamics of single fibrils of other proteins and peptides,[63-64, 68] including Aβ(25-35) and Aβ(1-42),[61] which showed significant asymmetry of the growth rates whereby one of the fibril ends was found to grow considerably faster than the other end.

The majority of the growth rates of individual fibrils grown at identical conditions fall within 50% of the average for these conditions; rare measurements exceed the average by up to 500% (Fig. 4A). We tested whether the growth rate variability is due to the presence of different polymorphs in the population of fibrils that we studied (each growth rate data point in Figs. 2 B and C, 3 E – H, and 4A corresponds to an individual fibril end). Since distinct polymorphs are expected to grow with specific rates[14, 40] and the polymorph identity is preserved during growth,[40] we determined the variability of growth rates evaluated from the displacement of single fibrils. For this, we divided the time evolutions of several fibril end displacements, like those shown in Fig. 1F, into segments of five overlapping data points and evaluated the growth rate corresponding to each segment of the time course (Fig. 4B, inset). The resulting distributions of the growth rates of individual fibrils (Fig. 4B) are comparable to those of batches of fibrils grown under identical conditions (e.g., Fig. 2B). This correspondence suggests that the growth rate variability is not due to polymorph diversity. The similarity of the growth rates of fibrils with thickness between 2 and 4 nm to those of thicker fibrils (Fig. 3F) strongly suggests that the majority of the fibrils observed here belong to the same twofold symmetric polymorph adopted by the seeds generated in stirred solutions.

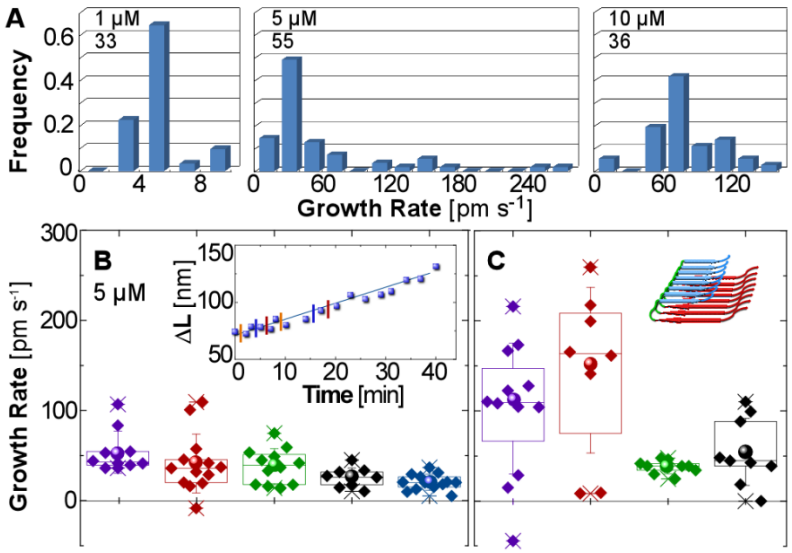

Figure 4. Variability of fibril growth rates. A. Distributions of fibril growth rates at Aβ40 concentrations indicated in the plots. Number of measurements indicated in each plot. **B and C.** Jitter plots (for definition of notations, please see caption of Fig. 2) of growth rate distributions of individual fibrils at the concentration indicated in B. **B.** Determined from the five displacement evolutions in Figure 1E. Color-coding corresponds to Figure 1E. Inset. Illustration of the determination of *R* from overlapping segments consisting of five points belonging to same displacement Δ*L* trace in B and C. Pairs of vertical bars of same color bracket Δ*L* data points used in individual determinations of *R*. **C.** Determined from the displacement evolutions of four fibrils of thickness between 2 and 4 nm. Inset. Schematic of a single protofilament that likely constitutes fibrils with thickness between 2 and 4 nm.

It appears that the growth rate variability is not due to interactions between adjacent protofilaments belonging to the same filament. To see this, we evaluated the variability in the growth rates of individual fibrils with thickness between 2 and 4 nm (Fig. 4C), and compared the degree of variability of these thin fibrils to that of thicker fibrils. We assume that the fibrils with measured thicknesses between 2 and 4 nm are single protofilaments. The variability of the growth rates for the thinnest fibrils (Fig. 4C) is comparable to or greater than that of thicker fibrils (Fig. 2B).

The growth rate fluctuations (Fig. 4 B and C) and the lack of cooperativity between the individual protofilaments comprising a fibril (Fig. 3F) may potentially lead to distinct lengths of the protofilaments and diminished fibril thickness close to the fibril end. We did not observe such

thickness variations. A feasible interpretation is that the rate fluctuations are around average values governed by the peptide concentration. Thus, over extended times, the adjacent protofilaments reach similar lengths and the potential length differences are likely lower than can be detected, given the resolution limit of the AFM of about 1 nm.

Steady or stop-and-go growth? Stop-and go-kinetics, in which periods of stagnation alternate with bursts of growth, have been observed in several previous studies of amyloid fibrillization at constant supersaturation.[61, 63, 69, 71] The most commonly cited molecular mechanism for stop-and-go kinetics is that a monomer docked at the fibril end adopts a conformation (before or during docking) that impedes further monomer attachment.[20, 98] Growth resumes after the capping monomer detaches or transitions to a conformation that more readily supports continued association.[61, 69, 71] The rest periods vary from several minutes to several hours and the lengths accrued between pauses reach between tens of nanometers and microns.[61, 63, 69, 71]

To discriminate more carefully between steady kinetics and stop-and-go kinetics, we chose a fibril oriented roughly along the scanning direction, which significantly enhances the resolution of the recorded displacement (Fig. 5A).[73] Previous meticulous measurements of the growth kinetics of a bacterial functional amyloid show that the pauses extend at lower supersaturation.[63] We therefore employed a relatively low concentration of Aβ40 of 1 μM to look for pauses. Over 18.5 min, the fibril grew by 4.8 nm, corresponding to an average growth rate of 4 pm s^{-1} (Fig. 5B). This evolution remained steady throughout the observation, at about 0.4 nm growth between images that were collected every 100 s (Fig. 5A). This steady growth does not represents a burst stage since the corresponding growth rate is similar to the average of 33 determinations with independently grown fibrils, summarized in Fig. 4A. In all, we monitored the growth of about 200 fibrils at five Aβ40 concentrations ranging from 1 to 10 μM. We never detected any significant periods of stalled growth. Fibril end displacements always evolved steadily, similar to those shown in Fig. 1E.

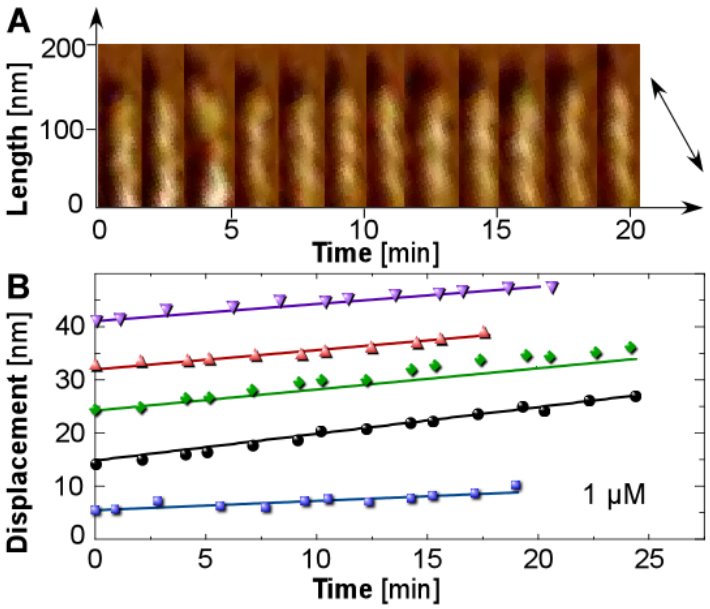

Figure 5. Steady growth of fibrils. A. A sequence of images of a fibril growing at 1 μM concentration aligned using an immobile set point to reveal the growth of the fibril. Double sided arrow indicates scanning direction. **B**. Evolutions of the displacement of the ends of five fibrils at Aβ40 concentration indicated in the plot. Bottom data set corresponds to the image sequence in A.

The present observation of relatively steady growth contrasts with the results of a detailed previous investigation that did exhibit stop-and-go growth of Aβ40 fibrils.[99] We believe the diverging observations may arise from two differences of the previous studies from the present approach: First, in the previous study the seeds of the fibrils that grew by discontinuous kinetics were generated in quiescent solutions, which, as highlighted above, favor threefold symmetric filaments.[14, 40] In contrast, the seeds we used were generated in agitated solutions, where mostly twofold symmetric filaments nucleate.[14, 40] Second, the previous studies monitored growth by total internal reflection fluorescent microcopy (TIRFM) in the presence of the dye Thioflavin T.[99] This dye may itself associate with the active fibrils ends, intermittently poisoning growth.

Growth reversibility and the rate constant for monomer association to the fibril. Fibrils placed in contact with buffer free of Aβ40 dissolve (Fig. 6 A – D) without stirring or agitation, demonstrating the reversibility of Aβ40 fibrillization. Similar to the growth of fibrils in

a supersaturated solution of the peptide, the dissolution of the fibrils occurs at a relatively steady rate (Fig. 6E). The correlation between the net fibril growth rate R and the Aβ40 concentration C in the range 0 – 10 μM is linear (Fig. 7A). The slope of the correlation, $(8.4\pm0.17) \times 10^{-3}$ nm s^{-1} μM^{-1}, is near the previously reported value for the twofold symmetric Aβ40 fibril polymorph of $(8.68\pm0.11) \times 10^{-3}$ nm s^{-1} μM^{-1}, determined by monitoring the evolution of the average length of fibrils grown in bulk solutions.[14] The respective slope for the three-fold symmetric polymorph, which was estimated in the same previous study, was lower, at 6.07 ± 0.23 nm s^{-1} μM^{-1}.[14] The close agreement between the kinetics measured here and determined previously for the twofold symmetric polymorph, as well as the significant difference with the threefold symmetric polymorph, provide additional support for our identification of the polymorph studied here as the twofold symmetric polymorph.

The $R(C)$ correlation crosses the line corresponding to zero growth at $C_e = 0.44 \pm 0.07$ μM, below which the negative values of R correspond to fibril dissolution (Fig. 7A). A solution with concentration C_e will thus be in equilibrium with the fibrils, so we can say C_e is the Aβ40 solubility

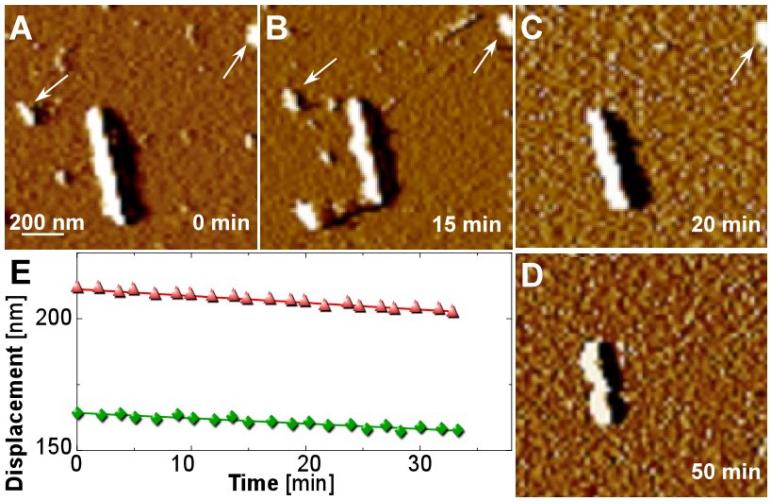

Figure 6. Characterization of Aβ40 fibril dissolution. A-D. Time-resolved *in situ* AFM images showing the dissolution of an Aβ40 fibril in peptide-free buffer. Arrows indicate immobile reference points. **E.** Evolutions of the displacements of two fibril ends and respective best-fit lines.

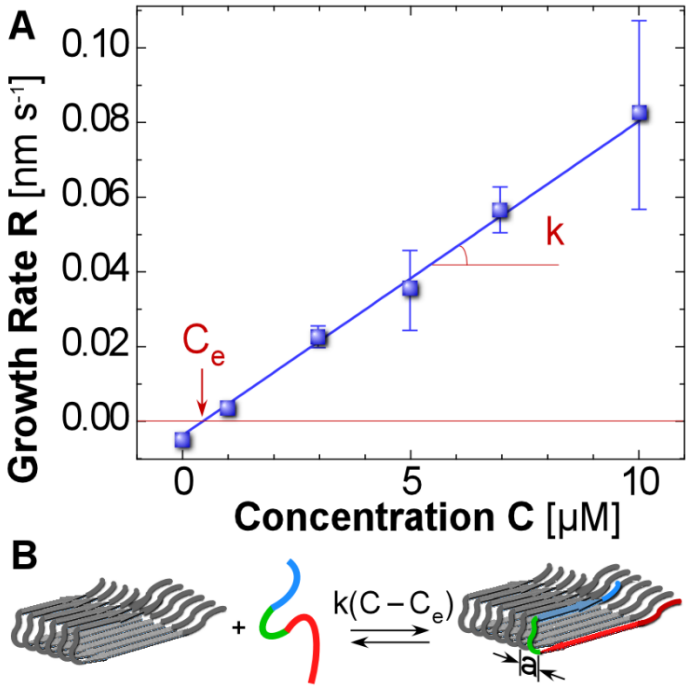

Figure 7. The correlation between fibril growth rate and Aβ40 concentration. A. Negative growth rates correspond to dissolution. The vertical arrow indicates the concentration at which the fibrils are in equilibrium with the solution, the solubility C_e. The slope of the best-fit line defines the rate constant k. Error bars indicate standard deviation from the average of 20 to 50 measurements at each concentration. **B.** Illustration of the relation between the net rate of monomer association to the fibril end $k_a(C - C_e)$ and the rate of fibril growth $R = ak_a(C - C_e)$.

with respect to the twofold symmetric fibril polymorph. The measured C_e is consistent with previous estimates of the solubility for the twofold symmetric Aβ40 fibril polymorph of 0.40 ± 0.04 μM and 0.34 ± 0.06 μM that were found, respectively, by following the time evolution of the average length of fibrils grown in bulk solutions and by measuring the concentration of peptide left in solution after fibril growth was completed.[14]

The apparent equilibrium between the fibrils and the solution should, of course, be regarded as metastable in view of the possible existence of more ordered condensed states, e.g., crystals or other polymorphs, which may have still lower free energy ΔG.[100] Even if such higher-order structures exist for AB40, they are kinetically avoided in the present study possibly owing to seeding with fibrils of a particular polymorph and the slow interconversion between different polymorphs. The ΔG difference between the fibrils studied here and a 1 M Aβ40 solution is the

standard free energy of fibrillization $\Delta G^o = -k_B N_A T \ln K = k_B N_A T \, ln C_e$= −36.5 kJ mol^{-1} = −8.7 kcal mol^{-1}, where k_B is the Boltzmann constant, N_A is the Avogadro number, T is temperature, and $K = C_e^{-1}$ = 2.3 μM^{-1} is the fibrillization equilibrium constant. This value for ΔG^o agrees with previous determinations.[101]

The measured dissolution rate is equal in magnitude to the growth rate recorded at a concentration with equivalent deviation from the equilibrium concentration (Fig. 7), implying that growth and dissolution are microscopically reversible. Microscopic reversibility would be violated if, for instance, growth occurred by monomer association, but the fibril were to dissolve, in contrast, by discharging dimers or other oligomers; the latter scenario would enforce asymmetric rates of growth and dissolution. The observed microscopic reversibility of fibril growth and dissolution represents a reference point for future models of fibril growth and dissolution.

The linear correlation between *R* and *C* suggests that the Aβ40 species that associates with the fibril during growth and that dissociates from the fibril during dissolution is a monomer. The net rate of growth of an individual fibril, *R*, at a given solution peptide concentration, *C*, represents the algebraic sum of the addition rate, R_a, and the dissociation rate, R_d. We assume that the rate of the unimolecular dissociation reaction, wherein a monomer leaves the fibril tip to yield a free monomer and a shorter fibril, is independent of the solution monomer concentration. Since only dissociation occurs in the absence of solution monomers, the dissolution rate at zero solution peptide concentration can be used to determine the intrinsic dissociation rate. The measured dissolution rate in the absence of solution monomers, R = −4.4 pm s^{-1}, can be converted into a dissociation rate of monomers from a single fiber end in units of molecules per second using the known spacing between monomers along the fibril axis, a = 0.47 nm (Fig. 7B).[84, 93-94] This conversion yields a dissociation rate of R_d = 9.4 × 10^{-3} molecules s^{-1} for a fibril end.

Supported by the linear $R(C)$ correlation, we assume that growth of fibrils occurs via the addition of monomers from the solution to an existing fibril end to yield a longer fibril. The rate of the bimolecular reaction between a monitored fibril end and solute monomers is proportional to the concentration of monomers in the solution, $R_a = k_a C$. If, rather than a single fiber study, we carried out a bulk experiment with many free fiber ends, the total rate would also be proportional to the concentration of these ends. When the solution monomer concentration is equal to the equilibrium concentration, $C = C_e = 0.44$ μM, the rates of dissociation and addition are equal in magnitude, $R_d = R_a(C_e) = k_a C_e$. With $R = a(R_a - R_d)$, the rate law corresponding to the linear $R(C)$ correlation (Fig. 7a) is $R = ak_a(C - C_e)$. Using the slope of the $R(C)$ correlation, 8.4× 10^{-3} nm s^{-1} μM^{-1}, and the spacing between monomers, a = 0.47 nm, we determine k_a = 1.8 × 10^4 M^{-1} s^{-1}. This value is well below the diffusion limit for reactions in solution of about 10^{10} $M^{-1}s^{-1}$, indicating that the monomer addition reaction is not diffusion-limited and a relatively large free energy barrier must be overcome to incorporate a monomer into a fibril. It therefore seems likely that the rate-limiting step of this reaction involves a conformational rearrangement that occurs from a pre-equilibrium where a monomer binds, but non-specifically, to the fibril tip before transforming into the next growth-competent fibril tip configuration, as has been suggested by previous theoretical work.[15, 19, 48, 80]

Conclusions. We have demonstrated that time-resolved *in situ* atomic force microcopy provides a way directly to measure the growth rates of individual Aβ40 fibrils without introducing complicating features that may confuse other commonly employed techniques. The ability faithfully to characterize the growth kinetics of individual amyloid fibrils provides an opportunity to explore the specific mechanistic details that control monomer association to fibrils.

We have identified the Aβ40 fibrils studied here as the twofold symmetric polymorph based on the good correspondence between the fibril growth rate constant to previous determinations for this polymorph. The population of fibrils includes not only single protofilaments but also

filaments and bundles of filaments. The growth rate, however, turns out to be independent of the fibril thickness, implying that adjacent protofilaments do not cooperate to assist or hamper monomer incorporation into their respective tips. Correspondingly, models of Aβ40 monomer association to single protofilaments may adequately describe the growth of thicker fibrils. The fibrils of the polymorph we studied grow steadily. The opposing ends of the fibrils grow with similar rates. These observations contrast with the "stop-and-go" kinetics and asymmetric growth that have been observed with amyloids formed from other peptide fragments or from Aβ40 whose seeds were generated differently and thus likely belong to the threefold symmetric polymorph.

The linear correlation between fibril growth rate and concentration suggests that the Aβ40 species that associates with the fibril during growth and dissociates from the fibril during dissolution is a monomer. Growth and dissolution of the Aβ40 amyloids are microscopically reversible, i.e., the sequence of molecular-level events leading to incorporation of a monomer to a fibril is exactly reversed during dissolution. The observed microscopic reversibility and unimolecular mechanisms of fibril growth and dissolution represent important reference points for models of fibril growth and dissolution.

The observed reversibility of fibrillization and symmetry of growth and dissolution allows the determination of the Aβ40 solubility with respect to the twofold symmetric fibril polymorph, as the interpolated concentration where the net rate of growth is zero. The solubility, C_e = 0.44 μM, and the standard free energy of fibrillization, ΔG^o = −36.5 kJ mol^{-1} = −8.7 kcal mol^{-1}, determined from the solubility, agree with previous determinations for the twofold symmetric polymorph.

The correlation between fibril growth rate and concentration corresponds to a rate coefficient for association of monomers to the fibril end k_a = 1.8×10^4 M^{-1}s^{-1}. This value is significantly slower than the diffusion limit implying that the transition state for incorporation of

a monomer into a fibril of the two-fold polymorph features a relatively high free energy. The rate-limiting step of this reaction may involve a conformational rearrangement of a monomer nonspecifically bound to the fibril tip to a growth-competent configuration, as suggested by previous models.

METHODS

We expressed Aβ(M1-40) (MDAEFRHDSGYEVHHQKLVFFAEDVGSNKGAIIGLMVGGV VIA) in *Escherichia coli* and purified it by size exclusion chromatography following published procedures.[102] The identity of the peptide was verified by western blot following the BIO-RAD protocol for polyclonal rabbit antibody. This method produces Aβ peptide with a methionine attached to the N-terminus, which significantly simplifies purification and contributes to several-fold greater yields.[102] Liquid chromatography-mass spectrometry (LC-MS, Figure S5) characterization of the purified peptide confirmed the identity of Aβ(M1-40) (M_w = 4,458.3 g mol^{-1} after correction for an added H^+) and revealed that about 0.1% of the total peptide is oxidized (M_w = 4,474.3 g mol^{-1}), probably at one of the two methionine sites, M0 or M35.[103-104] The fibrillization kinetics of the methionine-initiated peptide is quantitatively similar to that of the methionine-free peptide.[102] The recorded consistency may justify the wide use of Aβ(M1-40) and Aβ(M1-42) in amyloid β fibrillization studies.[12, 105] Our own determinations of both the solubility and the slope of the fibril growth rate correlation with the peptide concentration are very close to those recorded with synthetic Aβ(1-40), which lacks methionine.[14] Further details about the expression, purification, and validation of the peptide is provided in the Supporting Information.

The purified peptide was stored as a solution of concentration about 100 mM at -80°C. Aliquots of this stock solution were thawed, diluted to desired concentration, and used in AFM monitoring of the kinetics of fibril growth and dissolution within two hours.

We monitored the growth of fibrils deposited on mica by time-resolved *in situ* atomic force microscopy in solutions of desired peptide concentration. The temperature in the AFM fluid cell, 27.0 ± 0.1°C , was higher than room temperature (ca. 22°C) due to heating by the AFM scanner and laser. AFM images were collected in tapping mode. Image sizes ranged from 1 μm × 1 μm to 4 μm × 4 μm. Scan rates were between 1 and 2.52 s^{-1} in most images. Tests of the effects of tip speed on fibril growth employed scan rates of up to 10 s^{-1}. Height, amplitude, and phase imaging modalities of tapping-mode AFM were employed. The captured images contained 256 scan lines at angles depending on the orientation of the monitored fibril.[106-107] Thus, the collection of one image took approximately from 1:40 min to 4 min. The height images were used to determine the morphological characteristics of a fibril: thickness, length, integrity, etc. The corresponding amplitude images, in which the image intensity represents the deviation of the tip response frequency from the driving frequency due to interaction with the sample, were used for illustration of fibril growth. Note that the color density in amplitude imaging mode is not quantitatively related to sample height variations. A small fraction of the fibrils, less than 10%, fractured during imaging. Data collected with fractured fibrils were not include in subsequent analyses.

ASSOCIATED CONTENT

Supporting Information

The Supporting Information is available free of charge on the ACS Publications website.

Solution Preparation

Aβ40 Expression and Purification

LC-MS analysis

Fibril Formation

Time Resolved *in situ* Atomic Force Microscopy (AFM) imaging

ANOVA Test

Figures S1 – S8

Table S1

AUTHOR INFORMATION

Corresponding Authors

*vekilov@uh.edu; Phone: 713 743 4315.

*pwolynes@rice.edu; Phone: 713 348 4101.

ORCID

Peter G. Vekilov: 0000-0002-3424-8720

Author Contributions

Y.X., P.G.V., and P.G.W. conceived this project. P.G.V. and Y.X. designed research. Y.X. and M.S.S. expressed and purified the peptide. Y.X. and W.M carried out AFM characterization. Y.X. processed data. P.G.V., N.P.S., and P.G.W. proposed interpretations. P.G.V, N.P.S., and P.G.W wrote the paper.

Acknowledgements

We thank Christopher Pennington for the LC-MS characterization of the Aβ peptide and Dominque Maes and Vassiliy Lubchenko for valuable suggestions on the interpretation of the results presented here. This work was supported by NASA (Grants NNX14AE79G and NNX14AD68G to PGV), NSF (Grants MCB-1518204 and DMR-1710354 to PGV). Additional

support was provided by the Center for Theoretical Biological Physics at Rice University sponsored by NSF (Grant PHY-1427654 to PGW).

REFERENCES.

(1) 2017 Alzheimer's disease facts and figures. *Alzheimer's & Dementia* **2017,** *13* (4), 325-373.

(2) Hardy, J.; Allsop, D., Amyloid deposition as the central event in the aetiology of Alzheimer's disease. *Trends in Pharmacological Sciences* **1991,** *12*, 383-388.

(3) Hardy, J.; Higgins, G., Alzheimer's disease: the amyloid cascade hypothesis. *Science* **1992,** *256* (5054), 184-185.

(4) Selkoe, D. J., The molecular pathology of Alzheimer's disease. *Neuron* **1991,** *6* (4), 487-498.

(5) Haass, C.; Selkoe, D. J., Soluble protein oligomers in neurodegeneration: lessons from the Alzheimer's amyloid β-peptide. *Nature Reviews Molecular Cell Biology* **2007,** *8*, 101.

(6) Puzzo, D.; Gulisano, W.; Arancio, O.; Palmeri, A., The keystone of Alzheimer pathogenesis might be sought in Aβ physiology. *Neuroscience* **2015,** *307*, 26-36.

(7) Shankar, G. M.; Li, S.; Mehta, T. H.; Garcia-Munoz, A.; Shepardson, N. E.; Smith, I.; Brett, F. M.; Farrell, M. A.; Rowan, M. J.; Lemere, C. A.; Regan, C. M.; Walsh, D. M.; Sabatini, B. L.; Selkoe, D. J., Amyloid-β protein dimers isolated directly from Alzheimer's brains impair synaptic plasticity and memory. *Nature Medicine* **2008,** *14*, 837.

(8) Hubin, E.; van Nuland, N. A. J.; Broersen, K.; Pauwels, K., Transient dynamics of Aβ contribute to toxicity in Alzheimer's disease. *Cellular and Molecular Life Sciences* **2014,** *71* (18), 3507-3521.

(9) Kayed, R.; Head, E.; Thompson, J. L.; McIntire, T. M.; Milton, S. C.; Cotman, C. W.; Glabe, C. G., Common Structure of Soluble Amyloid Oligomers Implies Common Mechanism of Pathogenesis. *Science* **2003,** *300* (5618), 486-489.

(10) Sengupta, U.; Nilson, A. N.; Kayed, R., The Role of Amyloid-β Oligomers in Toxicity, Propagation, and Immunotherapy. *EBioMedicine* **2016,** *6*, 42-49.

(11) Panza, F.; Lozupone, M.; Logroscino, G.; Imbimbo, B. P., A critical appraisal of amyloid-β-targeting therapies for Alzheimer disease. *Nature Reviews Neurology* **2019,** *15* (2), 73-88.

(12) Cohen, S. I. A.; Cukalevski, R.; Michaels, T. C. T.; Šarić, A.; Törnquist, M.; Vendruscolo, M.; Dobson, C. M.; Buell, A. K.; Knowles, T. P. J.; Linse, S., Distinct thermodynamic signatures of oligomer generation in the aggregation of the amyloid-β peptide. *Nature Chemistry* **2018,** *10* (5), 523-531.

(13) Lu, J.-X.; Qiang, W.; Yau, W.-M.; Schwieters, Charles D.; Meredith, Stephen C.; Tycko, R., Molecular Structure of β-Amyloid Fibrils in Alzheimer's Disease Brain Tissue. *Cell* **2013,** *154* (6), 1257-1268.

(14) Qiang, W.; Kelley, K.; Tycko, R., Polymorph-Specific Kinetics and Thermodynamics of β-Amyloid Fibril Growth. *Journal of the American Chemical Society* **2013,** *135* (18), 6860-6871.

(15) Chen, M.; Schafer, N. P.; Wolynes, P. G., Surveying the Energy Landscapes of Aβ Fibril Polymorphism. *The Journal of Physical Chemistry B* **2018,** *122* (49), 11414-11430.

(16) Rodriguez, R. A.; Chen, L. Y.; Plascencia-Villa, G.; Perry, G., Thermodynamics of Amyloid-β Fibril Elongation: Atomistic Details of the Transition State. *ACS Chemical Neuroscience* **2018,** *9* (4), 783-789.

(17) Lin, Y.-C.; Li, C.; Fakhraai, Z., Kinetics of Surface-Mediated Fibrillization of Amyloid-β (12–28) Peptides. *Langmuir* **2018,** *34* (15), 4665-4672.

(18) Röder, K.; Wales, D. J., Energy Landscapes for the Aggregation of Aβ17–42. *Journal of the American Chemical Society* **2018,** *140* (11), 4018-4027.

(19) Zheng, W.; Tsai, M.-Y.; Wolynes, P. G., Comparing the Aggregation Free Energy Landscapes of Amyloid Beta(1–42) and Amyloid Beta(1–40). *Journal of the American Chemical Society* **2017,** *139* (46), 16666-16676.

(20) Bacci, M.; Vymětal, J.; Mihajlovic, M.; Caflisch, A.; Vitalis, A., Amyloid β Fibril Elongation by Monomers Involves Disorder at the Tip. *Journal of Chemical Theory and Computation* **2017,** *13* (10), 5117-5130.

(21) Schwierz, N.; Frost, C. V.; Geissler, P. L.; Zacharias, M., From Aβ Filament to Fibril: Molecular Mechanism of Surface-Activated Secondary Nucleation from All-Atom MD Simulations. *The Journal of Physical Chemistry B* **2017,** *121* (4), 671-682.

(22) Rojas, A.; Maisuradze, N.; Kachlishvili, K.; Scheraga, H. A.; Maisuradze, G. G., Elucidating Important Sites and the Mechanism for Amyloid Fibril Formation by Coarse-Grained Molecular Dynamics. *ACS Chemical Neuroscience* **2017,** *8* (1), 201-209.

(23) Elkins, M. R.; Wang, T.; Nick, M.; Jo, H.; Lemmin, T.; Prusiner, S. B.; DeGrado, W. F.; Stöhr, J.; Hong, M., Structural Polymorphism of Alzheimer's β-Amyloid Fibrils as Controlled by an E22 Switch: A Solid-State NMR Study. *Journal of the American Chemical Society* **2016,** *138* (31), 9840-9852.

(24) Economou, N. J.; Giammona, M. J.; Do, T. D.; Zheng, X.; Teplow, D. B.; Buratto, S. K.; Bowers, M. T., Amyloid β-Protein Assembly and Alzheimer's Disease: Dodecamers of Aβ42, but Not of Aβ40, Seed Fibril Formation. *Journal of the American Chemical Society* **2016,** *138* (6), 1772-1775.

(25) Schwierz, N.; Frost, C. V.; Geissler, P. L.; Zacharias, M., Dynamics of Seeded Aβ40-Fibril Growth from Atomistic Molecular Dynamics Simulations: Kinetic Trapping and Reduced Water Mobility in the Locking Step. *Journal of the American Chemical Society* **2016,** *138* (2), 527-539.

(26) Potapov, A.; Yau, W.-M.; Ghirlando, R.; Thurber, K. R.; Tycko, R., Successive Stages of Amyloid-β Self-Assembly Characterized by Solid-State Nuclear Magnetic Resonance with Dynamic Nuclear Polarization. *Journal of the American Chemical Society* **2015,** *137* (25), 8294-8307.

(27) Nasica-Labouze, J.; Nguyen, P. H.; Sterpone, F.; Berthoumieu, O.; Buchete, N.-V.; Coté, S.; De Simone, A.; Doig, A. J.; Faller, P.; Garcia, A.; Laio, A.; Li, M. S.; Melchionna, S.; Mousseau, N.; Mu, Y.; Paravastu, A.; Pasquali, S.; Rosenman, D. J.; Strodel, B.; Tarus, B.; Viles, J. H.; Zhang, T.; Wang, C.; Derreumaux, P., Amyloid β Protein and Alzheimer's Disease: When Computer Simulations Complement Experimental Studies. *Chemical Reviews* **2015,** *115* (9), 3518-3563.

(28) Qiang, W.; Akinlolu, R. D.; Nam, M.; Shu, N., Structural Evolution and Membrane Interaction of the 40-Residue β Amyloid Peptides: Differences in the Initial Proximity between Peptides and the Membrane Bilayer Studied by Solid-State Nuclear Magnetic Resonance Spectroscopy. *Biochemistry* **2014,** *53* (48), 7503-7514.

(29) Yates, E. A.; Legleiter, J., Preparation Protocols of Aβ(1–40) Promote the Formation of Polymorphic Aggregates and Altered Interactions with Lipid Bilayers. *Biochemistry* **2014,** *53* (45), 7038-7050.

(30) Lin, Y.-C.; Petersson, E. J.; Fakhraai, Z., Surface Effects Mediate Self-Assembly of Amyloid-β Peptides. *ACS Nano* **2014,** *8* (10), 10178-10186.

(31) Brännström, K.; Öhman, A.; Nilsson, L.; Pihl, M.; Sandblad, L.; Olofsson, A., The N-terminal Region of Amyloid β Controls the Aggregation Rate and Fibril Stability at Low pH Through a Gain of Function Mechanism. *Journal of the American Chemical Society* **2014,** *136* (31), 10956-10964.

(32) Nguyen, P.; Derreumaux, P., Understanding Amyloid Fibril Nucleation and Aβ Oligomer/Drug Interactions from Computer Simulations. *Accounts Chem. Res.* **2014,** *47* (2), 603-611.

(33) Härd, T., Amyloid Fibrils: Formation, Polymorphism, and Inhibition. *The Journal of Physical Chemistry Letters* **2014,** *5* (3), 607-614.

(34) Young, L. J.; Kaminski Schierle, G. S.; Kaminski, C. F., Imaging Aβ(1–42) fibril elongation reveals strongly polarised growth and growth incompetent states. *Physical Chemistry Chemical Physics* **2017,** *19* (41), 27987-27996.

(35) Liu, J.; Costantino, I.; Venugopalan, N.; Fischetti, R. F.; Hyman, B. T.; Frosch, M. P.; Gomez-Isla, T.; Makowski, L., Amyloid structure exhibits polymorphism on multiple length scales in human brain tissue. *Sci Rep* **2016,** *6*, 33079.

(36) Delgado, D. A.; Doherty, K.; Cheng, Q.; Kim, H.; Xu, D.; Dong, H.; Grewer, C.; Qiang, W., Distinct Membrane Disruption Pathways Are Induced by 40-Residue β-Amyloid Peptides. *Journal of Biological Chemistry* **2016,** *291* (23), 12233-12244.

(37) Watanabe-Nakayama, T.; Ono, K.; Itami, M.; Takahashi, R.; Teplow, D. B.; Yamada, M., High-speed atomic force microscopy reveals structural dynamics of amyloid β_{1–42} aggregates. *Proceedings of the National Academy of Sciences* **2016,** *113* (21), 5835-5840.

(38) Yang, C.-I.; Tsai, B. N. F.; Huang, S.-J.; Wang, T.-Y.; Tai, H.-C.; Chan, J. C. C., Aggregation of Beta-Amyloid Peptides Proximal to Zwitterionic Lipid Bilayers. *Chemistry – An Asian Journal* **2015,** *10* (9), 1967-1971.

(39) Ogi, H.; Fukukshima, M.; Hamada, H.; Noi, K.; Hirao, M.; Yagi, H.; Goto, Y., Ultrafast propagation of β-amyloid fibrils in oligomeric cloud. *Sci Rep* **2014,** *4*, 6960.

(40) Tycko, R., Physical and structural basis for polymorphism in amyloid fibrils. *Protein Sci.* **2014,** *23* (11), 1528-1539.

(41) Niu, Z.; Zhang, Z.; Zhao, W.; Yang, J., Interactions between amyloid β peptide and lipid membranes. *Biochimica et Biophysica Acta (BBA) - Biomembranes* **2018,** *1860* (9), 1663-1669.

(42) Niu, Z.; Zhao, W.; Zhang, Z.; Xiao, F.; Tang, X.; Yang, J., The Molecular Structure of Alzheimer β-Amyloid Fibrils Formed in the Presence of Phospholipid Vesicles. *Angewandte Chemie International Edition* **2014,** *53* (35), 9294-9297.

(43) Matsuzaki, K., Physicochemical interactions of amyloid β-peptide with lipid bilayers. *Biochimica et Biophysica Acta (BBA) - Biomembranes* **2007,** *1768* (8), 1935-1942.

(44) Knudsen, K. A.; Rosand, J.; Karluk, D.; Greenberg, S. M., Clinical diagnosis of cerebral amyloid angiopathy: Validation of the Boston Criteria. *Neurology* **2001,** *56* (4), 537-539.

(45) Nilsberth, C.; Westlind-Danielsson, A.; Eckman, C. B.; Condron, M. M.; Axelman, K.; Forsell, C.; Stenh, C.; Luthman, J.; Teplow, D. B.; Younkin, S. G.; Näslund, J.; Lannfelt, L., The 'Arctic' APP mutation (E693G) causes Alzheimer's disease by enhanced Aβ protofibril formation. *Nature Neuroscience* **2001,** *4* (9), 887-893.

(46) Grabowski, T. J.; Cho, H. S.; Vonsattel, J. P. G.; Rebeck, G. W.; Greenberg, S. M., Novel amyloid precursor protein mutation in an Iowa family with dementia and severe cerebral amyloid angiopathy. *Annals of Neurology* **2001,** *49* (6), 697-705.

(47) Päiviö, A.; Jarvet, J.; Gräslund, A.; Lannfelt, L.; Westlind-Danielsson, A., Unique Physicochemical Profile of β-Amyloid Peptide Variant Aβ1–40E22G Protofibrils: Conceivable Neuropathogen in Arctic Mutant Carriers. *Journal of Molecular Biology* **2004,** *339* (1), 145-159.

(48) Zheng, W.; Tsai, M.-Y.; Chen, M.; Wolynes, P. G., Exploring the aggregation free energy landscape of the amyloid-β protein (1–40). *Proceedings of the National Academy of Sciences* **2016,** *113* (42), 11835-11840.

(49) Lee, J.; Culyba, E. K.; Powers, E. T.; Kelly, J. W., Amyloid-β forms fibrils by nucleated conformational conversion of oligomers. *Nature Chemical Biology* **2011,** *7*, 602.

(50) Lee, C.-T.; Terentjev, E. M., Mechanisms and rates of nucleation of amyloid fibrils. *The Journal of Chemical Physics* **2017,** *147* (10), 105103.

(51) Sasmal, S.; Schwierz, N.; Head-Gordon, T., Mechanism of Nucleation and Growth of Aβ40 Fibrils from All-Atom and Coarse-Grained Simulations. *The Journal of Physical Chemistry B* **2016,** *120* (47), 12088-12097.

(52) Takami, M.; Nagashima, Y.; Sano, Y.; Ishihara, S.; Morishima-Kawashima, M.; Funamoto, S.; Ihara, Y., γ-Secretase: Successive Tripeptide and Tetrapeptide Release from the Transmembrane Domain of β-Carboxyl Terminal Fragment. *The Journal of Neuroscience* **2009,** *29* (41), 13042-13052.

(53) Kukar, T. L.; Ladd, T. B.; Robertson, P.; Pintchovski, S. A.; Moore, B.; Bann, M. A.; Ren, Z.; Jansen-West, K.; Malphrus, K.; Eggert, S.; Maruyama, H.; Cottrell, B. A.; Das, P.; Basi, G. S.; Koo, E. H.; Golde, T. E., Lysine 624 of the Amyloid Precursor Protein (APP) Is a Critical Determinant of Amyloid β Peptide Length: Support for a Sequential Model of ♈o-Secretase Intramembrane Proteolysis and Regulation by The Amyloid β Precursor Protein (APP) Juxtamembrane Region. *Journal of Biological Chemistry* **2011,** *286* (46), 39804-39812.

(54) Bitan, G.; Kirkitadze, M. D.; Lomakin, A.; Vollers, S. S.; Benedek, G. B.; Teplow, D. B., Amyloid β-protein (Aβ) assembly: Aβ40 and Aβ42 oligomerize through distinct pathways. *Proceedings of the National Academy of Sciences* **2003,** *100* (1), 330-335.

(55) Jarrett, J. T.; Lansbury, P. T., Seeding "one-dimensional crystallization" of amyloid: A pathogenic mechanism in Alzheimer's disease and scrapie? *Cell* **1993,** *73* (6), 1055-1058.

(56) Gravina, S. A.; Ho, L.; Eckman, C. B.; Long, K. E.; Otvos, L.; Younkin, L. H.; Suzuki, N.; Younkin, S. G., Amyloid β Protein (Aβ) in Alzheimeri's Disease Brain:Biochemical and Immunocytochemical Analysis with Antibodies Specific for Forms Ending At Aβ40 or Aβ42. *Journal of Biological Chemistry* **1995,** *270* (13), 7013-7016.

(57) Iwatsubo, T.; Odaka, A.; Suzuki, N.; Mizusawa, H.; Nukina, N.; Ihara, Y., Visualization of Aβ42(43) and Aβ40 in senile plaques with end-specific Aβ monoclonals: Evidence that an initially deposited species is Aβ42(43). *Neuron* **1994,** *13* (1), 45-53.

(58) Biancalana, M.; Koide, S., Molecular Mechanism of Thioflavin-T Binding to Amyloid Fibrils. *Biochimica et biophysica acta* **2010,** *1804* (7), 1405-1412.

(59) Hamley, I. W., The Amyloid Beta Peptide: A Chemist's Perspective. Role in Alzheimer's and Fibrillization. *Chemical Reviews* **2012,** *112* (10), 5147-5192.

(60) Persichilli, C.; Hill, S. E.; Mast, J.; Muschol, M., Does Thioflavin-T Detect Oligomers Formed During Amyloid Fibril Assembly. *Biophysical Journal* **2011,** *100* (3), 538-538.

(61) Kellermayer, M. S. Z.; Karsai, Á.; Benke, M.; Soós, K.; Penke, B., Stepwise dynamics of epitaxially growing single amyloid fibrils. *Proceedings of the National Academy of Sciences* **2008,** *105* (1), 141-144.

(62) Huang, Q.; Wang, H.; Gao, H.; Cheng, P.; Zhu, L.; Wang, C.; Yang, Y., In Situ Observation of Amyloid Nucleation and Fibrillation by FastScan Atomic Force Microscopy. *The Journal of Physical Chemistry Letters* **2019,** *10* (2), 214-222.

(63) Sleutel, M.; Van den Broeck, I.; Van Gerven, N.; Feuillie, C.; Jonckheere, W.; Valotteau, C.; Dufrêne, Y. F.; Remaut, H., Nucleation and growth of a bacterial functional amyloid at single fiber resolution. *Nature chemical biology* **2017,** *13* (8), 902-908.

(64) Goldsbury, C.; Kistler, J.; Aebi, U.; Arvinte, T.; Cooper, G. J. S., Watching amyloid fibrils grow by time-lapse atomic force microscopy. *Journal of Molecular Biology* **1999,** *285* (1), 33-39.

(65) Blackley, H. K. L.; Sanders, G. H. W.; Davies, M. C.; Roberts, C. J.; Tendler, S. J. B.; Wilkinson, M. J., In-situ atomic force microscopy study of β-amyloid fibrillization11Edited by M. F. Moody. *Journal of Molecular Biology* **2000,** *298* (5), 833-840.

(66) Hoyer, W.; Cherny, D.; Subramaniam, V.; Jovin, T. M., Rapid Self-assembly of α-Synuclein Observed by In Situ Atomic Force Microscopy. *Journal of Molecular Biology* **2004,** *340* (1), 127-139.

(67) Ban, T.; Hamada, D.; Hasegawa, K.; Naiki, H.; Goto, Y., Direct Observation of Amyloid Fibril Growth Monitored by Thioflavin T Fluorescence. *Journal of Biological Chemistry* **2003,** *278* (19), 16462-16465.

(68) Pinotsi, D.; Buell, A. K.; Galvagnion, C.; Dobson, C. M.; Kaminski Schierle, G. S.; Kaminski, C. F., Direct Observation of Heterogeneous Amyloid Fibril Growth Kinetics via Two-Color Super-Resolution Microscopy. *Nano Letters* **2014,** *14* (1), 339-345.

(69) Wördehoff, M. M.; Bannach, O.; Shaykhalishahi, H.; Kulawik, A.; Schiefer, S.; Willbold, D.; Hoyer, W.; Birkmann, E., Single Fibril Growth Kinetics of α-Synuclein. *Journal of Molecular Biology* **2015,** *427* (6, Part B), 1428-1435.

(70) Patil, S. M.; Mehta, A.; Jha, S.; Alexandrescu, A. T., Heterogeneous Amylin Fibril Growth Mechanisms Imaged by Total Internal Reflection Fluorescence Microscopy. *Biochemistry* **2011,** *50* (14), 2808-2819.

(71) Ferkinghoff-Borg, J.; Fonslet, J.; Andersen, C. B.; Krishna, S.; Pigolotti, S.; Yagi, H.; Goto, Y.; Otzen, D.; Jensen, M. H., Stop-and-go kinetics in amyloid fibrillation. *Physical Review E* **2010,** *82* (1), 010901.

(72) Tesei, G.; Hellstrand, E.; Sanagavarapu, K.; Linse, S.; Sparr, E.; Vácha, R.; Lund, M., Aggregate Size Dependence of Amyloid Adsorption onto Charged Interfaces. *Langmuir* **2018,** *34* (4), 1266-1273.

(73) Ruggeri, F. S.; Šneideris, T.; Vendruscolo, M.; Knowles, T. P. J., Atomic force microscopy for single molecule characterisation of protein aggregation. *Archives of Biochemistry and Biophysics* **2019,** *664*, 134-148.

(74) Maslova, M. V.; Gerasimova, L. G.; Forsling, W., Surface Properties of Cleaved Mica. *Colloid Journal* **2004,** *66* (3), 322-328.

(75) Schlichting, H.; Gersten, K., *Boundary layer theory, 8th Edition*. 8th ed.; Springer Verlag: Berlin, 2000.

(76) Dobson, J.; Kumar, A.; Willis, L. F.; Tuma, R.; Higazi, D. R.; Turner, R.; Lowe, D. C.; Ashcroft, A. E.; Radford, S. E.; Kapur, N.; Brockwell, D. J., Inducing protein aggregation by extensional flow. *Proceedings of the National Academy of Sciences* **2017,** *114* (18), 4673-4678.

(77) Ashton, L.; Dusting, J.; Imomoh, E.; Balabani, S.; Blanch, E. W., Shear-Induced Unfolding of Lysozyme Monitored In Situ. *Biophysical Journal* **2009,** *96* (10), 4231-4236.

(78) Ashton, L.; Dusting, J.; Imomoh, E.; Balabani, S.; Blanch, E. W., Susceptibility of Different Proteins to Flow-Induced Conformational Changes Monitored with Raman Spectroscopy. *Biophysical Journal* **2010,** *98* (4), 707-714.

(79) Coles, M.; Bicknell, W.; Watson, A. A.; Fairlie, D. P.; Craik, D. J., Solution structure of amyloid beta-peptide(1-40) in a water-micelle environment. Is the membrane-spanning domain where we think it is? *Biochemistry* **1998,** *37* (31), 11064-11077.

(80) Zheng, W. H.; Schafer, N. P.; Davtyan, A.; Papoian, G. A.; Wolynes, P. G., Predictive energy landscapes for protein-protein association. *Proceedings of the National Academy of Sciences of the United States of America* **2012,** *109* (47), 19244-19249.

(81) Byington, M. C.; Safari, M. S.; Conrad, J. C.; Vekilov, P. G., Protein Conformational Flexibility Enables the Formation of Dense Liquid Clusters: Tests Using Solution Shear. *The Journal of Physical Chemistry Letters* **2016,** *7*, 2339-2345.

(82) Byington, M. C.; Safari, M. S.; Conrad, J. C.; Vekilov, P. G., Shear flow suppresses the volume of the nucleation precursor clusters in lysozyme solutions. *J. Cryst. Growth* **2017,** *468*, 493-501.

(83) Qiang, W.; Yau, W.-M.; Lu, J.-X.; Collinge, J.; Tycko, R., Structural variation in amyloid-β fibrils from Alzheimer's disease clinical subtypes. *Nature* **2017,** *541*, 217.

(84) Petkova, A. T.; Leapman, R. D.; Guo, Z.; Yau, W.-M.; Mattson, M. P.; Tycko, R., Self-Propagating, Molecular-Level Polymorphism in Alzheimer's ß-Amyloid Fibrils. *Science* **2005,** *307* (5707), 262-265.

(85) Fändrich, M.; Meinhardt, J.; Grigorieff, N., Structural polymorphism of Alzheimer Abeta and other amyloid fibrils. *Prion* **2009,** *3* (2), 89-93.

(86) Fändrich, M.; Schmidt, M.; Grigorieff, N., Recent progress in understanding Alzheimer's β-amyloid structures. *Trends in Biochemical Sciences* **2011,** *36* (6), 338-345.

(87) Chen, B.; Thurber, K. R.; Shewmaker, F.; Wickner, R. B.; Tycko, R., Measurement of amyloid fibril mass-per-length by tilted-beam transmission electron microscopy. *Proceedings of the National Academy of Sciences* **2009,** *106* (34), 14339-14344.

(88) Fitzpatrick, A. W. P.; Debelouchina, G. T.; Bayro, M. J.; Clare, D. K.; Caporini, M. A.; Bajaj, V. S.; Jaroniec, C. P.; Wang, L.; Ladizhansky, V.; Müller, S. A.; MacPhee, C. E.; Waudby, C. A.; Mott, H. R.; De Simone, A.; Knowles, T. P. J.; Saibil, H. R.; Vendruscolo, M.; Orlova, E. V.; Griffin, R. G.; Dobson, C. M., Atomic structure and hierarchical assembly of a cross-β amyloid fibril. *Proceedings of the National Academy of Sciences* **2013,** *110* (14), 5468-5473.

(89) Pellarin, R.; Schuetz, P.; Guarnera, E.; Caflisch, A., Amyloid Fibril Polymorphism Is under Kinetic Control. *Journal of the American Chemical Society* **2010,** *132* (42), 14960-14970.

(90) Lomont, J. P.; Rich, K. L.; Maj, M.; Ho, J.-J.; Ostrander, J. S.; Zanni, M. T., Spectroscopic Signature for Stable β-Amyloid Fibrils versus β-Sheet-Rich Oligomers. *The Journal of Physical Chemistry B* **2018,** *122* (1), 144-153.

(91) Yau, S.-T.; Vekilov, P. G., Quasi-planar nucleus structure in apoferritin crystallisation. *Nature* **2000,** *406*, 494-497.

(92) Petsev, D. N.; Thomas, B. R.; Yau, S.-T.; Vekilov, P. G., Interactions and Aggregation of Apoferritin Molecules in Solution: Effects of Added Electrolytes. *Biophysical J.* **2000,** *78*, 2060-2069.

(93) Paravastu, A. K.; Leapman, R. D.; Yau, W.-M.; Tycko, R., Molecular structural basis for polymorphism in Alzheimer's β-amyloid fibrils. *Proceedings of the National Academy of Sciences* **2008,** *105* (47), 18349-18354.

(94) Goldsbury, C.; Frey, P.; Olivieri, V.; Aebi, U.; Müller, S. A., Multiple Assembly Pathways Underlie Amyloid-β Fibril Polymorphisms. *Journal of Molecular Biology* **2005,** *352* (2), 282-298.

(95) Iadanza, M. G.; Jackson, M. P.; Radford, S. E.; Ranson, N. A., MpUL-multi: Software for Calculation of Amyloid Fibril Mass per Unit Length from TB-TEM Images. *Sci Rep* **2016,** *6*, 21078-21078.

(96) Vekilov, P., Sickle-cell haemoglobin polymerisation: is it the primary pathogenic event of sickle-cell anaemia? *Brit. J. Haematol.* **2007,** *139* (2), 173-184.

(97) Galkin, O.; Nagel, R. L.; Vekilov, P. G., The kinetics of nucleation and growth of sickle cell hemoglobin fibers. *J. Mol. Biol.* **2007,** *365* (2), 425-439.

(98) Ilie, I. M.; Caflisch, A., Disorder at the Tips of a Disease-Relevant Aβ42 Amyloid Fibril: A Molecular Dynamics Study. *The Journal of Physical Chemistry B* **2018,** *122* (49), 11072-11082.

(99) Ban, T.; Hoshino, M.; Takahashi, S.; Hamada, D.; Hasegawa, K.; Naiki, H.; Goto, Y., Direct Observation of Aβ Amyloid Fibril Growth and Inhibition. *Journal of Molecular Biology* **2004,** *344* (3), 757-767.

(100) Reynolds, N. P.; Adamcik, J.; Berryman, J. T.; Handschin, S.; Zanjani, A. A. H.; Li, W.; Liu, K.; Zhang, A.; Mezzenga, R., Competition between crystal and fibril formation in molecular mutations of amyloidogenic peptides. *Nature Communications* **2017,** *8* (1), 1338.

(101) O'Nuallain, B.; Shivaprasad, S.; Kheterpal, I.; Wetzel, R., Thermodynamics of Aβ(1–40) Amyloid Fibril Elongation. *Biochemistry* **2005,** *44* (38), 12709-12718.

(102) Walsh, D. M.; Thulin, E.; Minogue, A. M.; Gustavsson, N.; Pang, E.; Teplow, D. B.; Linse, S., A facile method for expression and purification of the Alzheimer's disease-associated amyloid beta-peptide. *The FEBS journal* **2009,** *276* (5), 1266-1281.

(103) Aliyan, A.; Kirby, B.; Pennington, C.; Martí, A. A., Unprecedented Dual Light-Switching Response of a Metal Dipyridophenazine Complex toward Amyloid-β Aggregation. *Journal of the American Chemical Society* **2016,** *138* (28), 8686-8689.

(104) Aliyan, A.; Paul, T. J.; Jiang, B.; Pennington, C.; Sharma, G.; Prabhakar, R.; Martí, A. A., Photochemical Identification of Molecular Binding Sites on the Surface of Amyloid-β Fibrillar Aggregates. *Chem* **2017,** *3* (5), 898-912.

(105) Tesei, G.; Hellstrand, E.; Sanagavarapu, K.; Linse, S.; Sparr, E.; Vácha, R.; Lund, M., Aggregate Size Dependence of Amyloid Adsorption onto Charged Interfaces. *Langmuir : the ACS journal of surfaces and colloids* **2018,** *34* (4), 1266-1273.

(106) Olafson, K. N.; Ketchum, M. A.; Rimer, J. D.; Vekilov, P. G., Molecular Mechanisms of Hematin Crystallization from Organic Solvent. *Crystal Growth & Design* **2015,** *15* (11), 5535-5542.

(107) Olafson, K. N.; Ketchum, M. A.; Rimer, J. D.; Vekilov, P. G., Mechanisms of hematin crystallization and inhibition by the antimalarial drug chloroquine. *Proceedings of the National Academy of Sciences* **2015,** *112* (16), 4946-4951.